THE JOURNAL OF PHYSICAL CHEMISTRY Letters

Letter

Cite This: J. Phys. Chem. Lett. 2018, 9, 4355−4359

pubs.acs.org/JPCL

Fully Atomistic Real-Time Simulations of Transient Absorption Spectroscopy

Franco P. Bonafé,[†,‡] Federico J. Hernández,[†,‡] Bálint Aradi,[§] Thomas Frauenheim,[§] and Cristián G. Sánchez*[,†,‡]

[†]Departamento de Química Teórica y Computacional, Facultad de Ciencias Químicas, Universidad Nacional de Córdoba, Córdoba, Argentina

[‡]Instituto de Investigaciones en Fisicoquímica de Córdoba, INFIQC (CONICET - Universidad Nacional de Córdoba), Córdoba, Argentina

[§]Bremen Center for Computational Materials Science, Universität Bremen, Bremen, Germany

Supporting Information

ABSTRACT: We have implemented an electron−nuclear real-time propagation scheme for the calculation of transient absorption spectra. When this technique is applied to the study of ultrafast dynamics of Soret-excited zinc(II) tetraphenylporphyrin in the subpicosecond time scale, quantum beats in the transient absorption caused by impulsively excited molecular vibrations are observed. The launching mechanism of such vibrations can be regarded as a displacive excitation of the zinc−pyrrole and pyrrole C−C bonds.

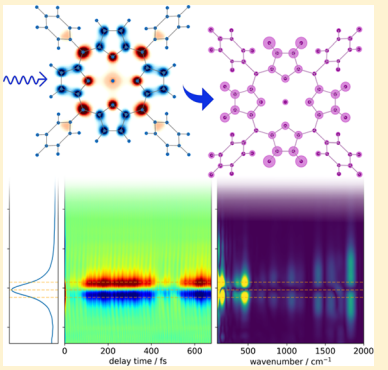

Computer simulations of femtosecond pump−probe spectroscopy experiments such as time-resolved photoabsorption have been a topic of interest of the scientific community for many years. In the last five years significant progress has been made in the development of atomistic techniques to simulate transient absorption (TA) of molecules in the time domain. De Giovannini et al. reported a protocol to compute the TA spectra in the attosecond time scale using time-dependent density functional theory (TDDFT) and applied to helium and ethylene.[1] Several issues and conditions regarding TDDFT exchange-correlation kernels were described and new methods that overcame the limitations of adiabatic TDDFT were published.[2−6] However, to the best of our knowledge, there is still no fully atomistic development that allows the simulation of TA spectra accounting for ion and electron dynamics after an initial perturbation (pump) to the electronic density.

Meanwhile, time-resolved broadband TA experiments using ultrashort (sub- or near-10-fs) pulses have been done to study ultrafast charge separation in organic systems,[7,8] photodynamics of DNA bases[9−11] and vibronic dynamics of retinal.[12] Sub-20-fs polaron-pair formation in an organic semiconductor was observed using such ultrashort pulses by two-dimensional spectroscopy.[13] In refs 7 and 8, ultrafast pump−probe spectroscopy was combined with TDDFT to understand charge separation in prototypical organic photovoltaic devices. Such ultrafast measurements of electronic−vibrational dynamics can shed light on important processes and be more directly compared with quantum-dynamical simulations on the subpicosecond regime.

Since the early 2000s, considerable debate has built up around zinc(II) tetraphenylporphyrin (ZnTPP). The seminal works lead by Gustavvson[14] and Zewail[15] of the ultrafast dynamics after photoexitacion of the Soret band roughly agreed on the decay lifetime of the S_2 excited state, which is between 1.5 and 2.4 ps depending on the solvent. A disagreement with the rise time of S_1 was reported by Zewail,[15] which suggested the existence of a dark state close to S_2. Further evidence proved that vibrational relaxation in the excited state (electronic-vibrational coupling) drives ultrafast relaxation dynamics instead of a dark state.[16] It would be interesting to understand, however, how and why such modes are launched in the first place.

In this letter we focus on the ultrafast (<700 fs) dynamics of ZnTPP after Soret band excitation with a resonant laser pulse by analyzing the time-resolved TA spectra, the vibrational signatures they contain, and the ion dynamics that accompanies the excitation by projecting into molecular normal modes.

Received: May 28, 2018
Accepted: July 19, 2018
Published: July 19, 2018

DOI: 10.1021/acs.jpclett.8b01659
J. Phys. Chem. Lett. 2018, 9, 4355−4359

Calculations are based on real-time (RT) Ehrenfest electron−ion dynamics within the density functional tight-binding (DFTB) formalism as implemented in the DFTB+ package.[17] DFTB is a very efficient semiempirical approach for quantum mechanical simulations based on a second order expansion of the Kohn−Sham energy functional around a reference density.[18] It has been successfully applied to study the real-time laser-driven dynamics of several metallic,[19,20] semiconductor[21] and molecular systems.[22−24]

TA spectra are calculated as follows. After a ground state electronic structure calculation, a time-dependent perturbation with a pulse shape (pump) is added to the Hamiltonian of the system, which allows for a real-time propagation of the one-electron reduced density matrix, by numerical integration of the Liouville−von Neumann equation for Ehrenfest dynamics within DFTB.[20] The instantaneous density matrix and atomic coordinates have all the necessary information to compute the absorption spectra at each time of the trajectory, so they are dumped to disk and a separate calculation is run, where a Dirac delta perturbation or *kick* (probe) to the instantaneous density matrix is applied and this trajectory is propagated keeping all the conditions of the simulation exactly as the original pump simulation. An effective linear response approach can be used to calculate the frequency-dependent polarizability $\alpha(\omega, \tau)$ (where τ is time difference between pump and probe, hereafter *delay time*) by Fourier transform of the dipole moment difference, as shown in eq 1. Here $\mu_P + p_\tau$ is the dipole moment of the system $\hat{\mu} = -e\hat{r}$ in the time-domain calculated after the probe kick at delay time τ and μ_P is the dipole moment of the simulation with the pump perturbation only.

$$\alpha(\omega, \tau) = \int \mathrm{d}t\ (\mu_{P+p_\tau}(t) - \mu_P(t+\tau))\exp(\mathrm{i}\omega t) \tag{1}$$

The absorption coefficient $\sigma(\omega)$ can be calculated from the polarizability as shown in eq 2. Due to the interference between the pump and the probe, a phase factor dependent on the delay time is introduced in the frequency-dependent polarizability, mixing the real and imaginary parts.[2] This contributions are not observed in typical pump−probe experiments where the signal is averaged over many laser shots. To get rid of such coherence we introduce a phase to the pump field and average the polarizability over four different phases, as described in ref 25. Thought this scheme increases the computational cost significantly, since it multiplies the number of calculations to be done by the number of phases, the use of TD-DFTB makes it feasible. The mathematical aspects of this method are out of the scope of this letter and will be explained in detail elsewhere.

$$\sigma(\omega) = \frac{4\pi\omega}{c}\,\mathrm{Im}(\alpha(\omega)) \tag{2}$$

ZnTPP's ground state absorption spectrum was calculated by RT propagation after a Dirac delta perturbation. The two lowest-energy active bands are the Q-band at 1.93 eV (642 nm) and the Soret or *B* band at 2.77 eV (447 nm), in relatively good agreement with the experimental values of 594 and 406 nm,[26] respectively, as expected for this method.[22] The system is then illuminated with a monochromatic $\sin^2$ pulse of pulse time t_p = 10 fs tuned to the Soret band energy and a peak field intensity of 0.02 V Å^{-1} (pump), yielding an energy fluence of 0.5 mJ cm^{-2}, and then evolves for 725 fs. During the dynamics, 2000 snapshots of the system's density matrix and geometry are stored, allowing us to calculate the TA spectra with a time resolution of 0.36 fs. In Figure 1 the differential absorption $\Delta A(\tau) = A(\tau) - A_{GS}$ is plotted for selected delay times: after

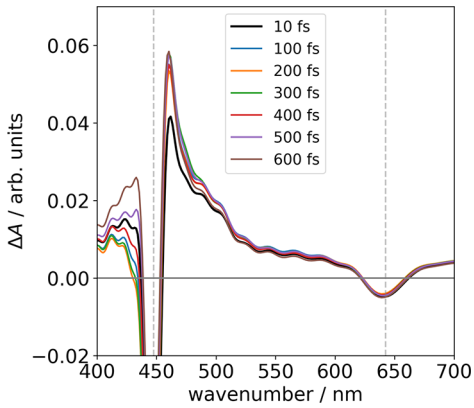

Figure 1. Differential absorption of ZnTPP ΔA for selected delay-times. The vertical dashed lines indicate the position of the Soret and Q bands.

the pump (τ = 10 fs) and every 100 fs. There is strong ground state bleaching (GSB) of the Soret and Q bands (indicated with a vertical dashed band) and a broad region of excited state absorption (ESA) to the red of the Soret band for λ > 470 nm, in agreement with experiments on ZnTPP measured in ethanol.[27,28] Similar ESA is observed in MgTPP and CdTPP.[29] The origin of such ESA band is not clear but it is likely absorption from S_1, since its intensity increases with time after pumping S_2 as it decays to S_1, while the GSB at the Q-band does not change significantly.[27]

The TA spectra are usually calculated subtracting the ground state spectrum; however, for the visualizations shown in this work (heatmaps) this quantity is not appropriate since the subtle changes that occur after the pulse are obscured by the strong bleach at the Soret band. Considering that the strongest changes to the absorption weights occur during the pump, it is better to calculate the absorption change with respect to the spectrum at the end of the pump (eq 3) and this is indeed what we show in the figures in this work.

$$\Delta A(t) = A(t) - A(t = t_p) \tag{3}$$

In Figure 2 the ground state and TA spectra are shown. The TA spectra calculated from electron−nuclear dynamics is depicted in Figure 1b. Around the Soret energy the signal is dominated by a strong ground state bleach, although this is ignored in the plot due to our choice of reference absorbance (*vide supra*, see Supporting Information, Figures S1 and S2); instead, the signal shows oscillatory features with changes in the sidebands of the Soret band and not in the peak center. In some experimental works, to study such oscillatory components the Fourier transform of the spectra along the delay time axis was calculated.[8,10−12] The fast Fourier transform of the TA spectra along each delay time is shown in Figure 1c. The spectral density shows significant peaks at wavenumbers around 200, 450, and 1800 cm^{-1} corresponding to periods of around 400, 74, and 18 fs. To investigate the cause of such oscillations the same simulation was performed clamping the nuclei and running the electron dynamics only; the TA spectra and spectral density are shown in Figure 1, parts d and e, respectively. No significant frequency components are detected

DOI: 10.1021/acs.jpclett.8b01659
J. Phys. Chem. Lett. 2018, 9, 4355−4359

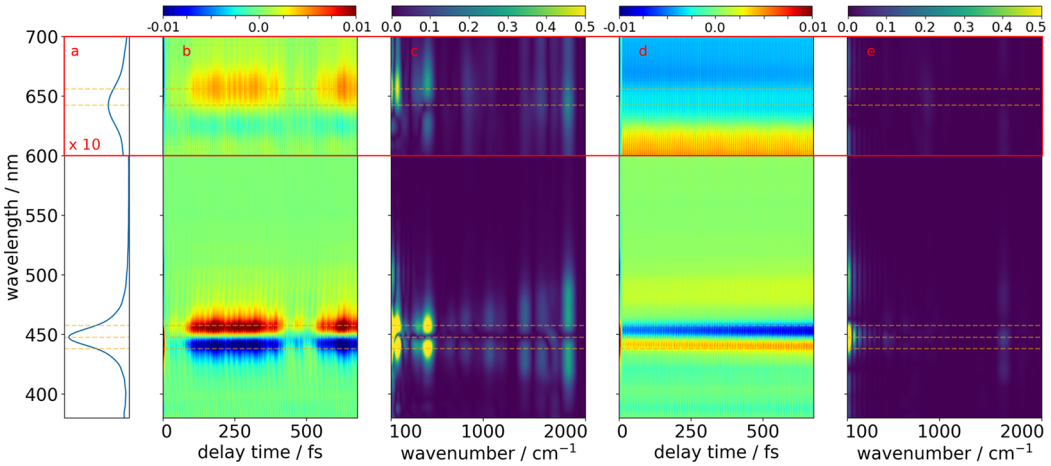

Figure 2. Ground state spectrum (a); TA spectra calculated by subtracting the absorption spectrum at each time with the spectrum at the time of the pulse for a simulation with moving (b) and clamped (d) ions; Fourier transform of the TA spectra along the delay time axis for moving (c) and clamped (e) ions. Dashed lines indicate the wavelength of the most important frequency contributions.

in this case, leading to the conclusion that such oscillations are of vibrational nature.

The effect on the Q-band is much weaker, as it can be seen in Figure 2. The frequency components of the spectral density are in agreement with those of the Soret band, although the low frequency oscillations are much stronger in the red sideband than in the blue.

A normal modes calculation in the ground state was performed by diagonalizing the mass-weighted Hessian matrix and the atomic coordinates along the evolution were projected onto the normal mode displacements (mass-weighted eigenvectors),[30] as shown in eq 4, where $\mathbf{v}_{Ai}$ is the eigenvectors matrix elements, $\Delta\mathbf{r}_A(t)$ are the nuclear displacements, m_A is the atomic mass and the coefficients Q_i thereby calculated are the coordinates in the normal mode basis. The potential energy of mode i can be calculated as shown on eq 5. The potential energy per mode was integrated along the trajectory and is depicted in Figure 3a, between 200 and 2000 cm^{-1}, while in parts b and c, the integrate spectral densities in the Soret region (between 280 and 520 nm) for moving and clamped ions are shown. The modes of 448 and 1830 cm^{-1} are the ones most coupled with the Soret transition, and can be identified as the symmetric zinc-pyrrole breathing (ZPB) mode and the symmetric pyrrole half-ring mode (PHR), respectively. These results partially agree with the experiments that were reported on this system after Soret excitation: the ZPB mode was identified at 388 cm^{-1} in ref 31. using chirped femtosecond pulses and resonance Raman spectra, and in ref 16 at 385 cm^{-1} using pump-degenerate four wave mixing and TA measurements; a high frequency mode was only assigned in ref 16 at 1352 cm^{-1} as the inner-ring stretch, which is compatible with a mode at 1405 cm^{-1} that is observed in our calculations (Figure 3b). In the energy per mode distribution there are also important contributions at low frequencies (below 200 cm^{-1}) that match the signals from the spectral density shown in Figure 2, although the trajectories are not long enough to resolve these peaks. Such very low-frequency modes would be strongly damped in experiment done in solution due to their nature, which involves motions that extend over the whole molecule and involve significant motion of the benzene rings.

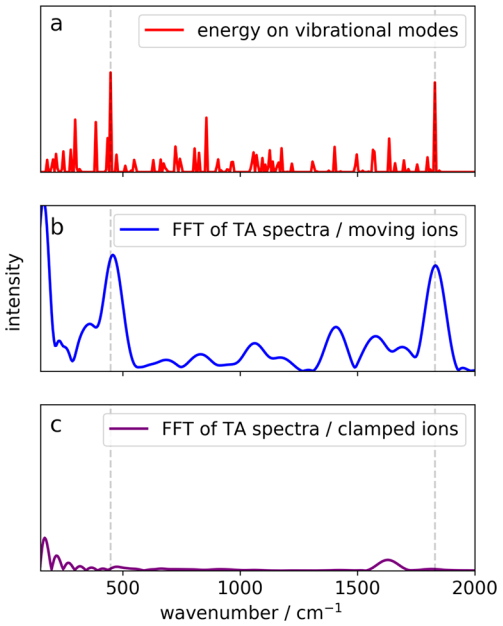

Figure 3. Total potential energy per mode (a); Fourier transform of TA spectra in the Soret region considering moving (b) and clamped (c) ions.

$$Q_i(t) = \sum_A m_A \Delta\mathbf{r}_A(t)\cdot\mathbf{v}_{Ai} \tag{4}$$

$$V_i(t) = (2\pi c\bar{\nu}_i Q_i(t))^2 \tag{5}$$

Interestingly, the usual approach to obtain the vibrational power spectrum from a molecular dynamics, namely the Fourier transform of the summed velocity−velocity autocorrelation function, did not yield the correct distribution of vibrational modes evidenced by the projection onto normal modes for nonequilibrium dynamics (see Figure S5 in the Supporting Information). Hence the simulated TA spectrum proves to be useful also as a computational tool to study optically driven impulsive vibrational dynamics.

None of the references above discuss the reasons for the selective excitation of the ZPB and PHR modes. Here we provide a geometrical interpretation based on an indirect

DOI: 10.1021/acs.jpclett.8b01659
J. Phys. Chem. Lett. 2018, 9, 4355−4359

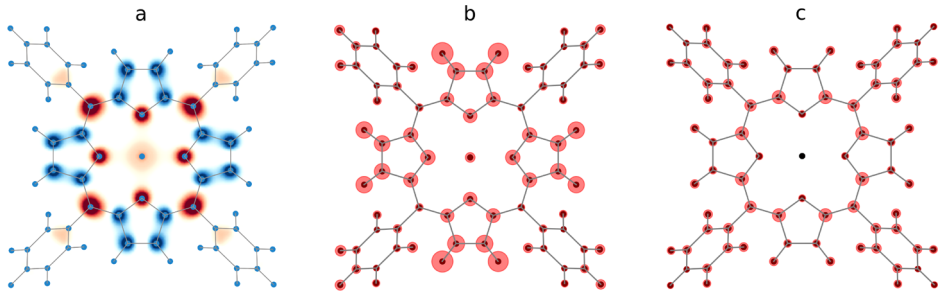

Figure 4. Transition density integrated over the *z* axis (a), where red and blue indicate density depletion and accumulation, respectively; magnitude of atomic displacements for the ZPB (b) and PHR (c) modes.

displacive mechanism. In Figure 4, the transition density for the Soret excitation integrated over the *z* axis along with the atomic displacements of the two most relevant modes that couple with this transition are shown. The transition density shows a density depletion region between the zinc and nitrogen atoms, and an accumulation between the pyrrole carbon atoms. This change of the bonding energy between the atoms launches nuclear motions in which the Zn−N distance increases and the pyrrole C−C distance stretches; once they reach their new equilibrium positions in the excited state surface, the motion continues by inertia, leading to an oscillatory motion which is compatible with the ZPB and PHR modes. This is known as *displacive excitation* of vibrational modes and has been reported as an important mechanism in molecular systems,[32] as well as semiconductor[33] and metallic nanoparticles.[20,34] A piece of evidence that supports this description is the increase in the oscillation amplitude with the increase of electrons excited to the levels above the Fermi energy (see Supporting Information, Figure S3), which is a known feature of displacive excitation.[33] In addition, a simulation with a longer pulse (50 fs) reveals selective excitation of the low frequency (ZPB) mode (see details in Figure S4), which confirms its impulsive character.

In summary, we have applied a new tool to the study of the vibrational motion launching and its electronic signature in a iconic system. Even though there are still limitations of the method to be overcome, such as the lack of inelastic dissipation of power to the vibrational degrees of freedom, it is remarkable that it is already possible to reproduce somewhat accurately the vibrational modes that are selectively excited and explain their origin from an atomistic time-dependent perspective.

■ ASSOCIATED CONTENT

Supporting Information

The Supporting Information is available free of charge on the ACS Publications website at DOI: 10.1021/acs.jpclett.8b01659.

Details regarding the choice of reference spectrum, the dependence of breathing mode excitation on pulse length, and the calculation of vibrational spectra (PDF)

■ AUTHOR INFORMATION

Corresponding Author

*(C.G.S.) E-mail: cgsanchez@fcq.unc.edu.ar.

ORCID

Franco P. Bonafé: 0000-0002-2069-6776

Cristián G. Sánchez: 0000-0001-7616-1802

Notes

The authors declare no competing financial interest.

■ ACKNOWLEDGMENTS

F.P.B. and F.J.H. thank CONICET for the doctoral and postdoctoral fellowships. The authors thank DFG-RTG2247 for the funding and the BCCMS for the computational resourcing provided.

■ REFERENCES

(1) De Giovannini, U.; Brunetto, G.; Castro, A.; Walkenhorst, J.; Rubio, A. Simulating Pump-Probe Photoelectron and Absorption Spectroscopy on the Attosecond Timescale with Time-Dependent Density Functional Theory. *ChemPhysChem* **2013**, *14*, 1363−1376.

(2) Perfetto, E.; Stefanucci, G. Some Exact Properties of the Nonequilibrium Response Function for Transient Photoabsorption. *Phys. Rev. A: At., Mol., Opt. Phys.* **2015**, *91*, 033416.

(3) Provorse, M. R.; Habenicht, B. F.; Isborn, C. M. Peak-Shifting in Real-Time Time-Dependent Density Functional Theory. *J. Chem. Theory Comput.* **2015**, *11*, 4791−4802.

(4) Fischer, S. A.; Cramer, C. J.; Govind, N. Excited State Absorption from Real-Time Time-Dependent Density Functional Theory. *J. Chem. Theory Comput.* **2015**, *11*, 4294−4303.

(5) Fuks, J. I.; Luo, K.; Sandoval, E. D.; Maitra, N. T. Time-Resolved Spectroscopy in Time-Dependent Density Functional Theory: An Exact Condition. *Phys. Rev. Lett.* **2015**, *114*, 183002.

(6) Nguyen, T. S.; Koh, J. H.; Lefelhocz, S.; Parkhill, J. Black-Box, Real-Time Simulations of Transient Absorption Spectroscopy. *J. Phys. Chem. Lett.* **2016**, *7*, 1590−1595.

(7) Andrea Rozzi, C.; Maria Falke, S.; Spallanzani, N.; Rubio, A.; Molinari, E.; Brida, D.; Maiuri, M.; Cerullo, G.; Schramm, H.; Christoffers, J.; et al. Quantum Coherence Controls the Charge Separation in a Prototypical Artificial Light-Harvesting System. *Nat. Commun.* **2013**, *4*, 1602.

(8) Falke, S. M.; Rozzi, C. A.; Brida, D.; Maiuri, M.; Amato, M.; Sommer, E.; De Sio, A.; Rubio, A.; Cerullo, G.; Molinari, E.; et al. Coherent Ultrafast Charge Transfer in an Organic Photovoltaic Blend. *Science* **2014**, *344*, 1001−1005.

(9) Prokhorenko, V. I.; Picchiotti, A.; Pola, M.; Dijkstra, A. G.; Miller, R. J. D. New Insights Into the Photophysics of DNA Nucleobases. *J. Phys. Chem. Lett.* **2016**, *7*, 4445−4450.

(10) Xue, B.; Yabushita, A.; Kobayashi, T. Ultrafast Dynamics of Uracil and Thymine Studied Using a sub-10 fs Deep Ultraviolet Laser. *Phys. Chem. Chem. Phys.* **2016**, *18*, 17044−17053.

(11) Kobayashi, T.; Kida, Y. Ultrafast Spectroscopy with sub-10 fs Deep-Ultraviolet Pulses. *Phys. Chem. Chem. Phys.* **2012**, *14*, 6200.

(12) Schnedermann, C.; Muders, V.; Ehrenberg, D.; Schlesinger, R.; Kukura, P.; Heberle, J. Vibronic Dynamics of the Ultrafast All-trans to 13-cis Photoisomerization of Retinal in Channelrhodopsin-1. *J. Am. Chem. Soc.* **2016**, *138*, 4757−4762.

(13) De Sio, A.; Troiani, F.; Maiuri, M.; Réhault, J.; Sommer, E.; Lim, J.; Huelga, S. F.; Plenio, M. B.; Rozzi, C. A.; Cerullo, G.; et al.

DOI: 10.1021/acs.jpclett.8b01659
J. Phys. Chem. Lett. 2018, 9, 4355−4359

Tracking the Coherent Generation of Polaron Pairs in Conjugated Polymers. *Nat. Commun.* **2016**, *7*, 13742.
(14) Gurzadyan, G. G.; Tran-Thi, T.-H.; Gustavsson, T. Time-Resolved Fluorescence Spectroscopy of High-Lying Electronic States of Zn-tetraphenylporphyrin. *J. Chem. Phys.* **1998**, *108*, 385−388.
(15) Yu, H. Z.; Baskin, J. S.; Zewail, A. H. Ultrafast Dynamics of Porphyrins in the Condensed Phase: II. Zinc Tetraphenylporphyrin. *J. Phys. Chem. A* **2002**, *106*, 9845−9854.
(16) Abraham, B.; Nieto-Pescador, J.; Gundlach, L. Ultrafast Relaxation Dynamics of Photoexcited Zinc-Porphyrin: Electronic-Vibrational Coupling. *J. Phys. Chem. Lett.* **2016**, *7*, 3151−3156.
(17) Aradi, B.; Hourahine, B.; Frauenheim, T. DFTB+, a Sparse Matrix-Based Implementation of the DFTB Method. *J. Phys. Chem. A* **2007**, *111*, 5678−5684.
(18) Elstner, M.; Porezag, D.; Jungnickel, G.; Elsner, J.; Haugk, M.; Frauenheim, T.; Suhai, S.; Seifert, G. Self-Consistent-Charge Density-Functional Tight-Binding Method for Simulations of Complex Materials Properties. *Phys. Rev. B: Condens. Matter Mater. Phys.* **1998**, *58*, 7260−7268.
(19) Douglas-Gallardo, O. A.; Berdakin, M.; Sánchez, C. G. Atomistic Insights into Chemical Interface Damping of Surface Plasmon Excitations in Silver Nanoclusters. *J. Phys. Chem. C* **2016**, *120*, 24389−24399.
(20) Bonafé, F. P.; Aradi, B.; Guan, M.; Douglas-Gallardo, O. A.; Lian, C.; Meng, S.; Frauenheim, T.; Sánchez, C. G. Plasmon-Driven Sub-Picosecond Breathing of Metal Nanoparticles. *Nanoscale* **2017**, *9*, 12391−12397.
(21) Fuertes, V. C.; Negre, C. F. A.; Oviedo, M. B.; Bonafé, F. P.; Oliva, F. Y.; Sánchez, C. G. A Theoretical Study of the Optical Properties of Nanostructured TiO2. *J. Phys.: Condens. Matter* **2013**, *25*, 115304−115311.
(22) Oviedo, M. B.; Negre, C. F. A.; Sánchez, C. G. Dynamical Simulation of the Optical Response of Photosynthetic Pigments. *Phys. Chem. Chem. Phys.* **2010**, *12*, 6706.
(23) Medrano, C. R.; Oviedo, M. B.; Sánchez, C. G. Photoinduced Charge-Transfer Dynamics Simulations in Noncovalently Bonded Molecular Aggregates. *Phys. Chem. Chem. Phys.* **2016**, *18*, 14840−14849.
(24) Mansilla Wettstein, C.; Bonafé, F. P.; Oviedo, M. B.; Sánchez, C. G. Optical Properties of Graphene Nanoflakes: Shape Matters. *J. Chem. Phys.* **2016**, *144*, 224305.
(25) Seidner, L.; Stock, G.; Domcke, W. Nonperturbative Approach to Femtosecond Spectroscopy: General Theory and Application to Multidimensional Nonadiabatic Photoisomerization Processes. *J. Chem. Phys.* **1995**, *103*, 3998−4011.
(26) Edwards, L.; Dolphin, D.; Gouterman, M.; Adler, A. Porphyrins XVII. Vapor Absorption Spectra and Redox Reactions: Tetraphenylporphins and Porphin. *J. Mol. Spectrosc.* **1971**, *38*, 16−32.
(27) Lukaszewicz, A.; Karolczak, J.; Kowalska, D.; Maciejewski, A.; Ziolek, M.; Steer, R. P. Photophysical Processes in Electronic States of Zinc Tetraphenyl Porphyrin Accessed on One- and Two-Photon Excitation in the Soret Region. *Chem. Phys.* **2007**, *331*, 359−372.
(28) Li, X.; Gong, C.; Gurzadyan, G. G.; Gelin, M. F.; Liu, J.; Sun, L. Ultrafast Relaxation Dynamics in Zinc Tetraphenylporphyrin Surface-Mounted Metal Organic Framework. *J. Phys. Chem. C* **2018**, *122*, 50−61.
(29) Liang, Y.; Bradler, M.; Klinger, M.; Schalk, O.; Balaban, M. C.; Balaban, T. S.; Riedle, E.; Unterreiner, A.-N. Ultrafast Dynamics of meso-Tetraphenylmetalloporphyrins: The Role of Dark States. *ChemPlusChem* **2013**, *78*, 1244−1251.
(30) Horiuchi, T.; Go, N. Projection of Monte Carlo and Molecular Dynamics Trajectories onto the Normal Modes Axes. *Proteins: Struct., Funct., Genet.* **1991**, *10*, 106−116.
(31) Yoon, M. C.; Jeong, D. H.; Cho, S.; Kim, D.; Rhee, H.; Joo, T. Ultrafast Transient Dynamics of Zn(II) Porphyrins: Observation of Vibrational Coherence by Controlling Chirp of Femtosecond Pulses. *J. Chem. Phys.* **2003**, *118*, 164−171.
(32) Wei, Z.; Li, J.; Wang, L.; See, S. T.; Jhon, M. H.; Zhang, Y.; Shi, F.; Yang, M.; Loh, Z.-H. Elucidating the Origins of Multimode Vibrational Coherences of Polyatomic Molecules Induced by Intense Laser Fields. *Nat. Commun.* **2017**, *8*, 735.
(33) Zeiger, H. J.; Vidal, J.; Cheng, T. K.; Ippen, E. P.; Dresselhaus, G.; Dresselhaus, M. S. Theory for Displacive Excitation of Coherent Phonons. *Phys. Rev. B: Condens. Matter Mater. Phys.* **1992**, *45*, 768−778.
(34) Varnavski, O.; Ramakrishna, G.; Kim, J.; Lee, D.; Goodson, T. Optically Excited Acoustic Vibrations in Quantum-sized Monolayer-protected Gold Clusters. *ACS Nano* **2010**, *4*, 3406−3412.

DOI: 10.1021/acs.jpclett.8b01659
J. Phys. Chem. Lett. 2018, 9, 4355−4359